

Photo-gating Carbon Nanotube Transistors

Matthew S. Marcus, J. M. Simmons, and O. M. Castellini

Department of Physics, University of Wisconsin - Madison

R. J. Hamers

Department of Chemistry, University of Wisconsin - Madison

M. A. Eriksson

Department of Physics, University of Wisconsin - Madison

Abstract

Optoelectronic measurements of carbon nanotube transistors have shown a wide variety of sensitivities to the incident light. Direct photocurrent processes compete with a number of extrinsic mechanisms. Here we show that visible light absorption in the silicon substrate generates a photovoltage that can electrically gate the nanotube device. The photocurrent induced by the changing gate voltage can be significantly larger than that due to direct electron-hole pair generation in the nanotube. The dominance of photogating in these devices is confirmed by the power and position dependence of the resulting photocurrent. The power dependence is strongly non-linear and photocurrents are measured through the device even when the laser illuminates up to 1 mm from the nanotube.

PACS numbers: 73.63.Fg, 78.67.Ch

I. INTRODUCTION

Since their discovery, carbon nanotubes have shown great promise for a wide variety of applications including nanoelectromechanical systems^{1,2} and chemical and biological sensing.^{3,4} The observation of photoconductivity in carbon nanotubes has opened a number of avenues of research in both characterization and photonic applications of nanotubes.^{5,6,7} Photocurrents have been used to characterize the electronic structure of nanotubes, such as the energies of van Hove singularities,^{7,8,9} as well as to image the Schottky barriers between a semiconducting nanotube and the metal contacts,¹⁰ and to build novel photodetectors using suspended nanotubes.¹¹ Recently, theory and experiments have shown that direct photogeneration of carriers is unable to explain the full photophysics of carbon nanotubes, and that excitonic^{12,13,14} and environmental (both substrate and gaseous)¹⁵ interactions must also be considered. An interesting feature of illuminating nanotube devices on a silicon/silicon dioxide substrate is that the silicon can also absorb light, leading to a voltage at the Si/SiO₂ interface. Such photo-voltages can, in many cases, be the dominant component of the induced photocurrent in nanotube devices. Understanding the interaction between the incident light, the back-gate, and the nanotube (photo)transistor is important both for potential applications of such devices, and to enable fundamental understanding of the direct nanotube-light interaction in nanotube transistors.

We show that photo-voltages in the silicon gate of carbon nanotube transistors have a significant impact on the measured photocurrent. The measured photocurrent is independent of laser polarization, indicating that direct electron-hole pair generation in the nanotube is negligible. We show that modulating the incident light effectively adds a small ac gate voltage, revealing the derivative of the source-drain current I_{ds} in the photocurrent. Comparing the numerical derivative of the I_{ds} vs. gate voltage curve taken without the light to the measured photocurrent as a function of gate voltage, we are able to extract the induced photovoltage which is typically on the order of -10 to -100 mV. Consistent with the photo-gating effect, the power and position dependence of the measured photocurrent is extremely non-linear. Indeed, photocurrents persist even when the laser illuminates up to 1 mm away from the nanotube position. The experiments are consistent with a theoretical analysis of the photo-gating mechanism. These measurements suggest that photo-voltages produced in transistor gates may provide the basis for unusual types of photo-detectors: devices in which

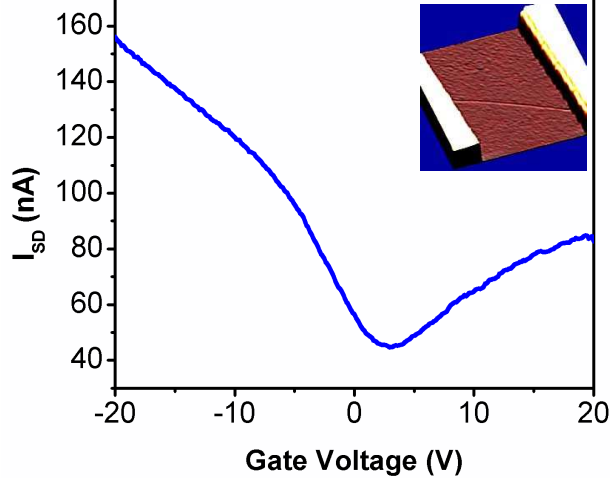


FIG. 1: Source-drain (I_{SD}) as a function of back gate voltage. The conduction through the nanotube increases at large values of both negative and positive gate voltages. Inset: AFM image of a $\sim 5 \mu\text{m}$ long single wall carbon nanotube transistor device.

the light absorbed by the gate produces a modulation in a transistor response, as opposed to the direct collection of photo-generated carriers in more conventional photo-detectors.

II. EXPERIMENTAL

The carbon nanotubes in the devices studied here are grown by chemical vapor deposition (CVD). Islands of nanotube catalyst are defined using electron-beam lithography,¹⁶ and the nanotubes are grown at 900 °C using a feedstock of methane (400 sccm) with a co-flow of hydrogen (20 sccm).^{17,18,19,20} The ends of the nanotube are buried under Ti/Au using electron-beam lithography in order to define the source-drain contacts. The nanotube channel and source-drain leads rest on top of a 500 nm thick SiO_2 layer that acts as a gate dielectric where the back gate is a heavily doped (nominally $\sim 10^{18} \text{ cm}^{-3}$) p-Si substrate. Nanotube transistors have been fabricated with both short ($\sim 5 \mu\text{m}$) and long ($\sim 500 \mu\text{m}$) channels. Fig. 1 is a plot of the source-drain current (I_{SD}) in a short channel device as a function of gate voltage under a fixed source-drain voltage ($V_{SD} = 250 \text{ mV}$). The conductance of the nanotube shown is dependent on the gate voltage, and it shows increased conductance at both positive and negative gate voltages. The gate dependence could indicate the presence of a semiconducting nanotube or may indicate effects of two nanotubes in

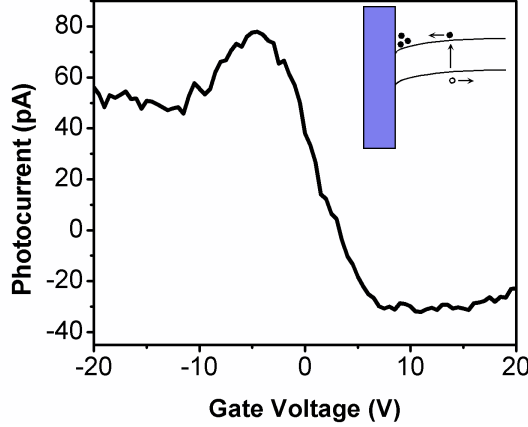


FIG. 2: Photocurrent measured through the nanotube channel as a function of gate voltage. The photocurrent switches sign near $V_g = 0$. Inset: Schematic of the energy bands with initial band bending at the Si/SiO₂ interface.

parallel, small metallic gap openings,²¹ or resonant electron scattering.^{22,23} Regardless of the origin of the gate dependence, all nanotubes that have a gate dependence can respond to photovoltages induced in the gate.

Nanotube devices are illuminated with a $P_o = 4$ mW HeNe laser that has a photon energy ($E_\gamma = 1.96$ eV) which is larger than both the band gap of our nanotubes²⁴ as well as the band gap of the Si gate ($E_{G,Si} = 1.12$ eV). For short channel devices the laser always illuminates the entire nanotube device, including the bulk of the nanotube and the metal-nanotube interface. The laser is modulated using an optical chopper and all photocurrents are measured with a lock-in amplifier referenced to the chopping frequency. When the signal is modulated with a chopper, the photo-voltage is a step function at the on or off transition, producing a capacitive spike in the current. Once the photo-voltage has reached a steady state and is not changing with respect to time, the capacitive current is zero. Slow modulation frequencies (10-100 Hz) are used in order to minimize the effects of capacitive coupling between the source-drain contacts and the gate during the turn on and turn off transitions.⁷

Photocurrents may arise from several sources. These include direct processes, such as electron-hole pairs generated in the nanotube, or indirect processes such as photo-desorption^{25,26} or photo-gating. The photocurrent for a nanotube transistor as a function of gate voltage is shown in Fig. 2 and, intriguingly, changes sign as a function of gate voltage.

Also, the photocurrent shows no dependence on the polarization of the laser with respect to the nanotube axis.^{7,10} The change in sign of the photocurrent in Fig. 2 and the absence of polarization dependence indicates that direct processes are not the source of the observed photocurrent. Direct photocurrent in a biased nanotube would have the same sign for all applied gate voltages because the electric field provided by the bias voltage would sweep all the photo-generated carriers in the same direction, independent of the gate voltage. Photo-desorption of oxygen from the metal-nanotube contacts also cannot account for the observed photocurrent. The removal of oxygen from the nanotube and/or contacts, thereby affecting the metal-nanotube Schottky barrier, would lead to decreased p-channel conductivity (negative gate voltages), and increased n-channel conductivity (positive gate voltages).²⁶ The data in Fig. 2 show an increase in p-channel conductivity, and a decrease in the n-channel conductivity, the opposite of what is expected for a photo-desorption process. Photo-gating, as we show below, can explain both the increased p-, and decreased n-channel conductivity as well as the observed sign change.

III. PHOTO-GATING MECHANISM

Photo-gating occurs when photo-excited charge in the silicon gate causes a change in potential (δV_{PV}) at the Si/SiO₂ interface. In order for photo-gating to occur, there needs to be a slope in the Si energy bands at the Si/SiO₂ interface. Bending in the Si energy bands provides an electric field that separates the electron-hole pairs produced by the laser and a potential well to trap either electrons or holes.^{27,28} Band bending is often present due to charge in the oxide (mobile ions, fixed charge, and interface states) which induces a depletion region near the Si/SiO₂ interface. In addition to the presence of band bending, to produce a significant photovoltage the potential well must be deep enough to act as a trap at the measurement temperature (~ 25 meV).

In order to determine if there is band bending at the Si/SiO₂ interface, capacitance-voltage (CV) characteristics of a metal-oxide-semiconductor capacitor (MOSC) are measured.^{29,30} The MOSC is fabricated on an oxidized Si wafer from the same batch as the nanotube samples studied. Fits to the experimental CV data (not shown) indicate that the bulk doping concentration is $N_a \approx 1.2 \times 10^{18} \text{ cm}^{-3}$, and that there is an offset voltage $\Delta V_o = -28 \text{ V}$. The non-zero offset voltage indicates the presence of initial band bending

due to oxide charge. If the offset voltage were zero there would be no curvature in the Si energy bands and therefore no photo-gating effect. The oxide charge density can be estimated using $N_{ox} \approx -C_{ox}\Delta V_o/e \approx 1.2 \times 10^{12} \text{ cm}^{-2}$ where C_{ox} is the capacitance per area of the oxide, and e is the magnitude of the electron charge. The positive oxide charge induces an equal negative charge in the silicon substrate ($Q_s = -N_{ox} \approx -1.2 \times 10^{12} \text{ cm}^{-2}$), such that the energy bands in the silicon are bent downwards, establishing a trap for photo-excited electrons.

In order to produce a photovoltage, the magnitude of the potential created as a result of oxide charge must be significant enough to provide an electric field that can redistribute the electron-hole pairs generated by the laser. The charge in the silicon is a function of the surface potential (band bending, see Fig. 3a) ϕ_s and is given by the expression²⁷

$$Q_s = -\sqrt{2k_B T \varepsilon_{Si} n_i} F(U_s, U_b, \Delta n) \quad (1)$$

where

$$\begin{aligned} F(U_s, U_b, \Delta n) = & [e^{U_b}(e^{-U_s} + U_s - 1) \\ & + e^{-U_b}(e^{U_s} - U_s - 1) \\ & + \Lambda e^{U_b}(e^{U_s} + e^{-U_s} - 2)]^{1/2} \end{aligned} \quad (2)$$

is the normalized interfacial electric field, assuming that the depletion width is smaller than the diffusion length, and that recombination currents can be ignored. In the previous equations k_B is Boltzmann's constant, T is temperature, ε_{Si} is the dielectric constant of Si, n_i is the intrinsic number of carriers, U_s and U_b are the normalized surface and bulk potential $U_s = q\phi_s/k_B T$, $U_b = \ln(N_a/n_i)$ and Λ is the ratio of photo-excited carriers to the equilibrium number of majority carriers $\Lambda = \Delta p/p_o = \Delta n/p_o$, also referred to as the injection ratio. Due to the complexity of Eq. 2, the magnitude of the potential is most easily found graphically or numerically. First, in the absence of light, $F(U_s, U_b, \Delta n)$ becomes a function only of the surface potential ϕ_s . Using the value of Q_s determined above, $F(U_s, U_b, \Delta n = 0) \equiv F_o$ is computed using Eq. 1. The value of F_o is shown as the dotted line in the inset of Fig. 4. Next, using Eq. 2, F is plotted as a function of ϕ_s and the intersection of the curve with the dotted line sets the initial amount of potential ϕ_{so} due to the oxide charge. For the MOSC, the potential ϕ_{so} , shown schematically in Fig. 3a, is measured to be $\sim 120 \text{ mV}$ which is

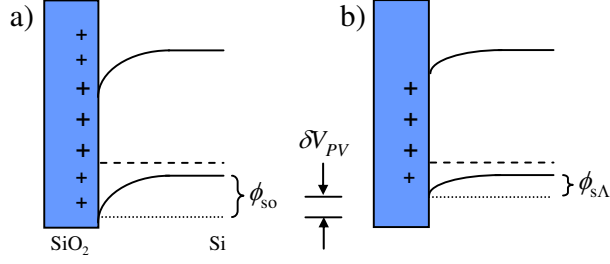


FIG. 3: Schematic band diagrams showing band bending ϕ_s in the silicon substrate for the as fabricated device (a) and under laser illumination (b). For typical oxide charge densities, the initial band bending ϕ_{so} is $\sim 100 - 200$ mV. Under illumination, the positive oxide charge is partially screened by photogenerated electrons that become trapped at the interface, reducing the surface potential from $\phi_{so} \rightarrow \phi_{s\Lambda}$. The resulting photovoltage δV_{PV} is given by Eq. 3.

larger than the thermal carrier energies, enabling photo-generated electrons to be trapped at the Si/SiO₂ interface.

Photo-excited electrons and holes in the silicon are separated by the interfacial electric field. This charge redistribution changes the potential in the silicon from ϕ_{so} to a different value $\phi_{s\Lambda}$ (Fig. 3b). The difference between the two potentials is the measured photo-voltage,

$$\delta V_{PV} = \phi_{s\Lambda} - \phi_{so}. \quad (3)$$

So long as the laser does not affect the amount of oxide charge, the total charge in the silicon remains constant and, according to Eq. 1, the value of F must stay fixed at F_o . When illumination causes Λ to become nonzero, U_s , and therefore ϕ_s , must change to keep $F = F_o$. The inset of Fig. 4 shows several different F vs. ϕ_s curves as the injection ratio Λ is varied. The potential under illumination $\phi_{s\Lambda}$ is the intersection point between the curve for a given Λ and the initial interfacial field F_o . For low values of the injection ratio, there are few photo-generated carriers to fill the potential well at the Si/SiO₂ interface, and $\phi_{s\Lambda} \approx \phi_{so}$. As the injection ratio is increased, there are more carriers to fill the well, and the bands become less curved, reaching flat-band conditions for high values of Λ . Thus, as the injection ratio increases, the measured photovoltage will change from 0 to $-\phi_{so}$. The magnitude of the resulting photo-voltage is plotted as a function of photo-carrier density in Fig. 4, using a bulk silicon doping density of $N_a \sim 1.2 \times 10^{18} \text{ cm}^{-3}$ ($\Delta n = \Lambda N_a$) and the measured initial surface potential $\phi_{so} \sim 120$ mV. Once the bands are flat ($\phi_{s\Lambda} = 0$),

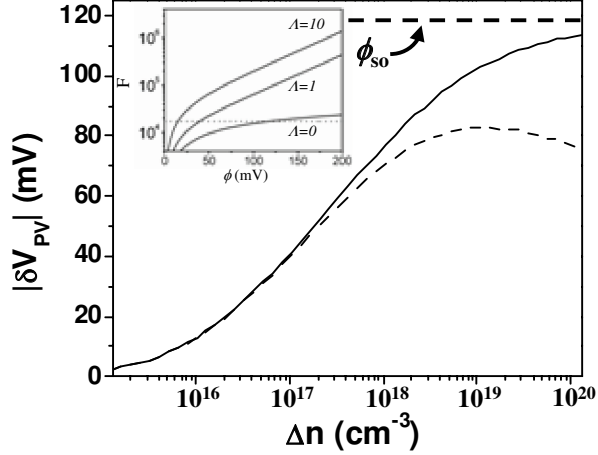


FIG. 4: Calculated magnitude of photovoltage as a function of the number of photo-excited carriers, assuming a bulk doping density of $N_a \approx 1.2 \times 10^{18} \text{ cm}^{-3}$ and an initial surface potential of $\phi_{so} \sim 120 \text{ mV}$. The solid line includes only the effect of the initial band bending. The dotted line includes the effect of the Demer voltage (see appendix). Inset: Calculated normalized electric field at the Si/SiO₂ interface as a function of the surface potential and injection ratio. The dotted line indicates the value of the field F_o as determined from the initial charge in the silicon Q_s .

there is no electric field to separate the electrons and holes and the measured photovoltage saturates. This is illustrated in Fig. 4 where the photovoltage asymptotically approaches ϕ_{so} when Λ becomes large, and in the inset where the interface potential tends to 0. It is important to note that since different processing conditions can lead to changes in the initial surface potential, photovoltages measured on different samples can have higher or lower values than the maximum presented in Fig. 4.²⁹ Also, for sufficiently high injection ratios ($\Delta n \gtrsim p_o$), other processes, such as the Demer voltage²⁸ presented in the appendix, can become important and could dominate over the photovoltage due to initial band curvature as shown by the dashed curve in Fig. 4. As we show next, we remain in the low-injection limit where these additional effects can be ignored.

In the limit of low-injection conditions, $\Delta n < p_o$, we can estimate the number of excited carriers as²⁷

$$\Delta n \approx \frac{I \alpha L_n}{(1 + \alpha L_n)(s_1 + D_n/L_n)} \lesssim 10^{17} \text{ cm}^{-3}, \quad (4)$$

where $\alpha \approx 3000 \text{ cm}^{-1}$ is the absorption coefficient³⁰ of Si at $\lambda = 633 \text{ nm}$, $D_n = 7 \text{ cm}^2/\text{s}$ is the minority carrier diffusion coefficient, $L_n = 45 \text{ } \mu\text{m}$ is the diffusion length, I is the

photon intensity, and s_1 is the surface recombination velocity at the Si/SiO₂ interface. The diffusion coefficient ($D_n = k_B T / q \mu_n$) and diffusion length ($L_n = \sqrt{D_n \tau_n}$) are calculated using the minority carrier recombination lifetime,³¹ $\tau_n = 3 \times 10^{-6}$ s, and the minority carrier drift mobility,³⁰ $\mu_n \sim 270$ cm²/Vs. The photon intensity is given by $I = \xi \eta (1 - R) 2 P_o / e E_\gamma \pi \omega^2$, where η is the quantum efficiency (assumed to be unity), $R = 0.5$ is the measured reflectivity of the Si, and $\omega \sim 20 \mu\text{m}$ is the estimated laser spot radius. The factor of $\xi = 0.2$ is used to account for the portion of the laser power incident on the underlying silicon that is not absorbed by the metal leads. The surface recombination velocity depends on a variety of factors including interface state density, gate voltage, and the number of photo-excited carriers,³² and is typically on the order of 100 – 1000 cm/s. As an order of magnitude estimate, we assume that s_1 is negligible, which is valid as long as $s_1 < D_n / L_n \approx 1500$ cm/s. Due to our approximations for s_1 and η , and because Eq. 4 does not account for diffusion of carriers parallel to the Si/SiO₂ interface, the calculated value is an over-estimate of the photo-excited carrier density. This over-estimate confirms that we are in the low-injection limit ($\Delta n < N_a \approx 10^{18}$ cm⁻³) for our experimental conditions. Using Δn and Fig. 4, the photo-voltage is estimated to be $\delta V_{PV} < -40$ mV. The actual photo-voltage measured in the experiment is extracted and is compared to this value later.

IV. DISCUSSION

The photo-voltage produced in the silicon gate couples into the nanotube circuit by providing an additional gate voltage for the nanotube channel. When the light is modulated, the effective gate voltage is $V_g = V_{DC} + \delta V_{PV}(t)$, where δV_{PV} is the time dependant photovoltage and V_{DC} is an existing gate voltage applied by a battery. Since the current in the channel is measured with a lock-in amplifier, the measured photocurrent is $I_{PC} = \frac{\partial I_{SD}}{\partial V_g} \delta V_{PV}$. Thus, the data shown in Fig. 2 may be understood as a derivative measurement of Fig. 1, and the photocurrent reveals the change in the source-drain current due to the addition of a small negative ac gate voltage to the existing dc gate voltage. From Fig. 1 we see that adding a small negative gate voltage to an existing negative gate voltage causes the source-drain current to increase, yielding a positive derivative and positive photocurrent. At positive gate voltages, the effect of adding a small negative gate voltage causes the source-drain current to decrease, yielding a negative photocurrent.

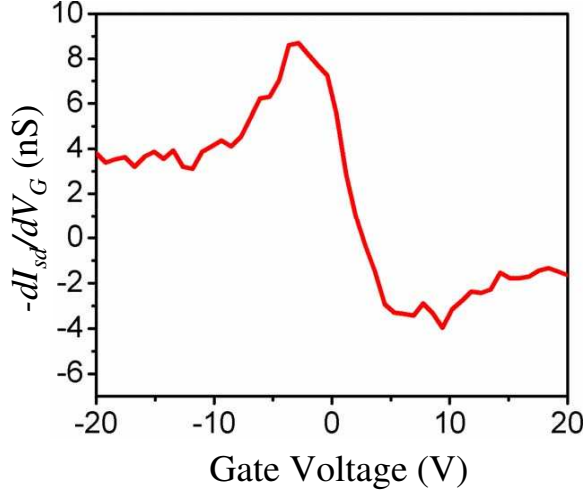


FIG. 5: Numerically calculated derivative from the data in Fig. 1. The form of the derivative is extremely similar to the measured photocurrent in Fig. 2 where the p-channel conduction is increased and the n-channel is suppressed.

The magnitude of the photo-gated photocurrent depends on both the nanotube-gate coupling $\frac{\partial I_{SD}}{\partial V_g}$ and the photo-voltage δV_{PV} at the Si/SiO₂ interface. The photo-voltage can be extracted by dividing the photocurrent signal by the gate derivative $\frac{\partial I_{SD}}{\partial V_g}$, which is calculated numerically from the data in Fig. 1 and is shown in Fig. 5. The photo-voltage for this device is $\delta V_{PV} = -15$ mV and is independent of the applied gate voltage. This measured value of photovoltage is similar to the over-estimate of calculated above, supporting the photogating mechanism.

The power dependence of the photocurrent is another important parameter for establishing the role of photo-gating. The generation rate of photo-carriers is linear with laser power, both in the nanotube and in the silicon. For a direct photocurrent process in the nanotube I_{PC} is expected to be proportional to the generation rate, whereas for photo-gating $I_{PC} \propto \delta V_{PV}$ which is non-linear in the number of excited carriers. Using neutral density filters to change the incident laser intensity, the photocurrent as a function of power was measured on a long channel nanotube device³³ and is shown in Fig. 6. Using the nanotube-gate coupling and the measured photocurrent, the induced photovoltage for this device was measured to be $\delta V_{PV} = -160$ mV. Similar to Fig. 4, the photocurrent changes logarithmically under low injection before saturating at high laser intensities.

It is interesting to note that the photo-voltage depends only weakly on where the laser

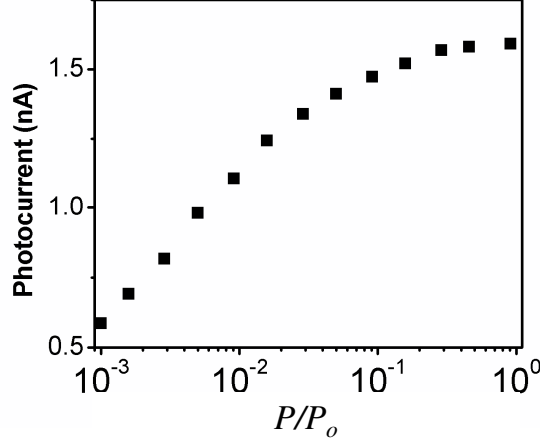


FIG. 6: Measured photocurrent as a function of the incident laser power on a long channel nanotube device. The non-linearity of the intensity dependence indicates that the photocurrent does not arise from a direct process.

illuminates the sample relative to the nanotube. This fact is illustrated in the upper inset to Fig. 7, which shows the photocurrent as a function of position perpendicular to the long axis of the nanotube at the position indicated by the arrow in the lower inset. The curve is slightly asymmetric about the position of the nanotube due to the proximity of the device to the edge of the silicon chip. The surprising feature of Fig. 7 is that there is an appreciable photocurrent, reduced only by a factor of ~ 3 , even when the laser spot is centered over 1 mm away from the device. Using a laser spot with an $\sim 60 \mu\text{m}$ gaussian width, there are virtually no carriers produced near the nanotube at such a large distance from the nanotube. Since the laser isn't producing carriers near the nanotube, the carriers must be mobile in the Si. Thus the photocurrent that is induced by the photovoltage arises from laser generated carriers near the nanotube as well as carriers that diffuse towards the nanotube. We can phenomenologically express the number of carriers under the nanotube as

$$\Delta n(x)/\Delta n_o = Ae^{-2x^2/\omega^2} + Be^{-|x|/L_n}, \quad (5)$$

where the first term accounts for direct photo-generation of carriers in the silicon under the nanotube, and the second term is from carriers generated at some distance from the nanotube diffusing towards the nanotube. Using Fig. 6 to relate the photocurrent to incident power, and since Δn is proportional to the laser power, we can relate the measured photocurrent to the ratio of $\Delta n(x)/\Delta n_o$, where Δn_o is the number of carriers generated in the silicon

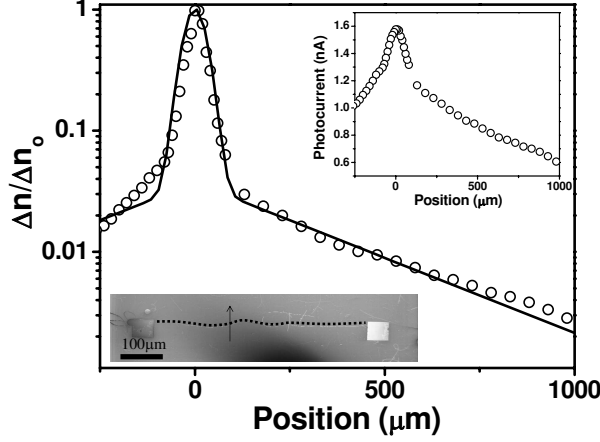


FIG. 7: Ratio of photo-generated electrons in the silicon substrate as a function of position. The circles are the experimentally measured values, extracted by relating the raw photocurrent vs. position in the upper inset to the intensity dependence shown in Fig. 6. The line is a fit to Eq. 5 which includes direct generation of carriers beneath the nanotube as well as diffusion of carriers when the laser illuminates away from the nanotube. Upper inset: Photocurrent as a function of position perpendicular to the long axis of nanotube. Photocurrent is measured up to 1 mm away from the nanotube. Lower inset: SEM image of the $\sim 500 \mu\text{m}$ nanotube device, where the dotted line indicates the position of the nanotube. The arrow shows the position and direction of the scanned laser.

at the photocurrent maxima. The solid line in Fig. 7 is a fit to the experimental data using equation Eq. 5, with the exponential prefactors A and B , the beam waist ω , and the diffusion length L_n as free parameters. The experimental data is well fit by Eq. 5 using $\omega = 58 \mu\text{m}$ and $L_n = 350 \mu\text{m}$. The extracted value of L_n is an effective diffusion length, as opposed to the bulk diffusion length, and can depend greatly on the detailed geometry and injection conditions that are present. These results illustrate that photo-gating is a long-range interaction. Carriers that are generated in the silicon substrate millimeters away from the nanotube still have a significant effect on the nanotube circuit.

Photo-gated nanotube devices present an interesting alternative to photo-detection on the nanoscale. Such a device would separate the absorption of photons from the detection current, such that each can be independently optimized. The gate material (silicon in this case) would determine the absorption properties of the detector, and could be modified to

increase the absorption cross-section at the desired wavelengths. The sensitivity of the photo-gated nanotube detector is determined by the nanotube-gate coupling $\frac{\partial I_{SD}}{\partial V_g}$, which may be custom tailored through device engineering of the Schottky barriers,³⁴ and geometry, as well as mode of operation (sub-threshold vs. on).³⁵ Nanotubes offer many properties that make them superior channel materials such as high mobilities³⁶ and large saturation velocities,³⁷ but there is no reason to expect that photo-gating of the type studied here should be unique to carbon nanotube channels.

In conclusion we have demonstrated that light absorption in the substrate of carbon nanotube field effect transistors generates an extra photo-voltage at the Si/SiO₂ interface. This photovoltage acts as an additional negative gate voltage of order 10-100 mV on the nanotube transistor and, depending on the magnitude of the nanotube-gate coupling, produces changes in the source-drain current of up to ~ 2 nA which is considerably larger than previously reported photocurrents in carbon nanotubes.^{7,8} The photo-voltage responds nonlinearly to the power in the laser beam, increasing only by a factor of 3 over three orders of magnitude in laser power, and is only weakly dependent on where the carriers are generated with respect to the nanotube. We find that charge generated in the Si substrate up to 1 mm away from the nanotube still produces a measurable photocurrent. The current due to photogating can, in many cases, be the dominant component of the photocurrent measured through nanotube transistors and must be accounted for in order to determine the intrinsic/direct photocurrent in nanotube devices. Though photogating complicates the analysis of photocurrent measurements, it also offers a different mode of photodetection where the absorption and detection elements are separate. This style of detection would allow for individual optimization of the photoabsorber and the electronic sensitivity of the transistor channel.

Acknowledgments

We would like to acknowledge Jennifer Sebbly-Strabley for useful discussions. We would also like to acknowledge funding from the NSF CAREER program under grant number DMR-0094063, the NSF MRSEC program under grant number DMR-0520527, and the NSF NSEC program under grant number DMR-0425880.

APPENDIX: DEMBER VOLTAGE

In addition to a potential forming from the redistribution of photo-excited charge, another voltage that can form in the substrate, the Dember voltage, is particularly relevant for high injection conditions where $\Delta n \gtrsim p_o$. The Dember voltage is produced when photo-excited electrons and holes diffuse at different rates. The differing diffusion rates lead to a separation of the charge, which in turn generates an electric field in the silicon substrate. Because the electron mobility is higher than the hole mobility in silicon, the sign of the Dember voltage is always positive and will appear in series with the band-induced photo-voltage, effectively reducing the total amount of photovoltage measured in the nanotube device. The Dember voltage is expressed as²⁸

$$V_d = \frac{k_B T}{e} \frac{b-1}{b+1} \ln \left[1 + \frac{(b+1)\Delta n}{n_o + bp_o} \right] \quad (\text{A.1})$$

where b is the ratio of electron to hole mobility $\mu_n/\mu_p \sim 1.8$ and n_o is the equilibrium number of electrons in the silicon. Using the over-estimated value of Δn from Eq. 4, the Dember voltage in our devices is $V_d \approx 1$ mV which is much less than the measured photo-voltage due to band curvature for the analysis presented here. For larger values of excited carriers, the Dember voltage can become comparable to the photo-voltage and should not be ignored. The effect of the Dember voltage is shown in Fig. 4, where the calculated total photovoltage for the case when there is only band curvature (solid line) is compared to when the Dember voltage is included (dotted line), assuming a bulk doping density of $N_a \approx 1.2 \times 10^{18} \text{ cm}^{-3}$ and initial band bending of $\phi_{so} = -120$ mV. As can be seen, the effect of the Dember voltage is small under low-injection conditions, but becomes sizable when the number of injected carriers nears the bulk doping density. It is important to note that both the band curvature and Dember voltages depend on the bulk doping and oxide charge densities and must be recalculated if higher or lower doping concentrations are used.

List of Figures:

1. Source-drain (I_{SD}) as a function of back gate voltage. The conduction through the nanotube increases at large values of both negative and positive gate voltages. Inset: AFM image of a $\sim 5 \mu\text{m}$ long single wall carbon nanotube transistor device.
2. Photocurrent measured through the nanotube channel as a function of gate voltage. The photocurrent switches sign near $V_g = 0$. Inset: Schematic of the energy bands with initial band bending at the Si/SiO₂ interface.
3. Schematic band diagrams showing band bending ϕ_s in the silicon substrate for the as fabricated device (a) and under laser illumination (b). For typical oxide charge densities, the initial band bending ϕ_{so} is $\sim 100 - 200$ mV. Under illumination, the positive oxide charge is partially screened by photogenerated electrons that become trapped at the interface, reducing the surface potential from $\phi_{so} \rightarrow \phi_{s\Lambda}$. The resulting photovoltage δV_{PV} is given by Eq. 3.
4. Calculated magnitude of photovoltage as a function of the number of photo-excited carriers, assuming a bulk doping density of $N_a \approx 1.2 \times 10^{18} \text{ cm}^{-3}$ and an initial surface potential of $\phi_{so} \sim 120$ mV. The solid line includes only the effect of the initial band bending. The dotted line includes the effect of the Dember voltage (see appendix). Inset: Calculated normalized electric field at the Si/SiO₂ interface as a function of the surface potential and injection ratio. The dotted line indicates the value of the field F_o as determined from the initial charge in the silicon Q_s .
5. Numerically calculated derivative from the data in Fig. 1. The form of the derivative is extremely similar to the measured photocurrent in Fig. 2 where the p-channel conduction is increased and the n-channel is suppressed.
6. Measured photocurrent as a function of the incident laser power on a long channel nanotube device. The non-linearity of the intensity dependence indicates that the

photocurrent does not arise from a direct process.

7. Ratio of photo-generated electrons in the silicon substrate as a function of position. The circles are the experimentally measured values, extracted by relating the raw photocurrent vs. position in the upper inset to the intensity dependence shown in Fig. 6. The line is a fit to Eq. 5 which includes direct generation of carriers beneath the nanotube as well as diffusion of carriers when the laser illuminates away from the nanotube. Upper inset: Photocurrent as a function of position perpendicular to the long axis of nanotube. Photocurrent is measured up to 1 mm away from the nanotube. Lower inset: SEM image of the $\sim 500 \mu\text{m}$ nanotube device, where the dotted line indicates the position of the nanotube. The arrow shows the position and direction of the scanned laser

-
- ¹ V. Sazonova, Y. Yaish, H. Üstünel, D. Roundy, T. A. Arias, and P. L. McEuen, *Nature* **431**, 284 (2004).
 - ² A. M. Fennimore, T. D. Yuzvinsky, W.-Q. Han, M. S. Fuhrer, J. Cumings, and A. Zettl, *Nature* **424**, 408 (2003).
 - ³ C. S. Lee, S. E. Baker, M. S. Marcus, W. Yang, M. A. Eriksson, and R. J. Hamers, *Nano Letters* **4**, 1713 (2004).
 - ⁴ A. Star, E. Tu, J. Niemann, J. C. P. Gabriel, C. S. Joiner, and C. Valcke, *Proceedings of the National Academy of Sciences* **103**, 921 (2006).
 - ⁵ A. Fujiwara, Y. Matsuoka, H. Suematsu, N. Ogawa, K. Miyano, H. Kataura, Y. Maniwa, S. Suzuki, and Y. Achiba, *Japanese Journal of Applied Physics* **40**, L1229 (2001).
 - ⁶ I. A. Levitsky and W. B. Euler, *Applied Physics Letters* **83**, 1857 (2003).
 - ⁷ M. Freitag, Y. Martin, J. A. Misewich, R. Martel, and Ph. Avouris, *Nano Letters* **3**, 1067 (2003).
 - ⁸ Y. Ohno, S. Kishimoto, T. Mizutani, T. Okazaki, and H. Shinohara, *Applied Physics Letters* **84**, 1368 (2004).
 - ⁹ A. Mohite, G. Sumanasekera, K. Hirahara, S. Bandow, S. Iijima, and B. Alphenaar, *Chemical Physics Letters* **412**, 190 (2005).
 - ¹⁰ K. Balasubramanian, Y. Fan, M. Burghard, K. Kern, M. Friedrich, U. Wannek, and A. Mews, *Applied Physics Letters* **84**, 2400 (2004).
 - ¹¹ H.-C. Yuan, B. Yang, J. M. Simmons, M. S. Marcus, Z. Ma, M. A. Eriksson, and M. G. Lagally, in *Photonic Applications in Nonlinear Optics, Nanophotonics, and Microwave Photonics* (SPIE, Toronto, Canada, 2005), vol. 5971, p. 597118.
 - ¹² E. J. Mele and C. L. Kane, *Solid State Communications* **135**, 527 (2005).
 - ¹³ Y. Z. Ma, L. Valkunas, S. M. Bachilo, and G. R. Fleming, *Journal of Physical Chemistry B* **109**, 15671 (2005).
 - ¹⁴ C.-X. Sheng, Z. V. Vardeny, A. B. Dalton, and R. H. Baughman, *Physical Review B* **71**, 125427 (2005).
 - ¹⁵ M. E. Itkis, F. Borondics, A. Yu, and R. C. Haddon, *Science* **312**, 413 (2006).
 - ¹⁶ J. Kong, H. T. Soh, A. M. Cassell, C. F. Quate, and H. Dai, *Nature* **395**, 878 (1998).
 - ¹⁷ Carbon nanotubes are grown in a FirstNano CVD system. FirstNano, Inc., 1860 Smithtown

- Ave., Ronkonkoma, NY 11779.
- ¹⁸ A. V. Melechko, V. I. Merkulov, T. E. McKnight, M. A. Guillorn, K. L. Klein, D. H. Lowndes, and M. L. Simpson, *Journal of Applied Physics* **97**, 041301 (2005).
 - ¹⁹ A. Moisala, A. G. Nasibulin, and E. I. Kauppinen, *Journal of Physics - Condensed Matter* **15**, S3011 (2003).
 - ²⁰ J. M. Simmons, B. M. Nichols, M. S. Marcus, O. M. Castellini, R. J. Hamers, and M. A. Eriksson, *Small* **2**, 902 (2006).
 - ²¹ M. Ouyang, J. L. Huang, C. L. Cheung, and C. M. Lieber, *Science* **292**, 702 (2001).
 - ²² M. Bockrath, W. Liang, D. Bozovic, J. H. Hafner, C. M. Lieber, M. Tinkham, and H. Park, *Science* **291**, 283 (2001).
 - ²³ D. Bozovic, M. Bockrath, J. H. Hafner, C. M. Lieber, H. Park, and M. Tinkham, *Physical Review B* **67**, 033407 (2003).
 - ²⁴ Nanotubes with diameters larger than ~ 0.5 nm have band gaps that are less than the photon energy of our laser.
 - ²⁵ R. J. Chen, N. R. Franklin, J. Kong, J. Cao, T. W. Tombler, Y. Zhang, and H. Dai, *Applied Physics Letters* **79**, 2258 (2001).
 - ²⁶ M. Shim and G. P. Siddons, *Applied Physics Letters* **83**, 3564 (2003).
 - ²⁷ D. K. Schroder, *Measurement Science and Technology* **12**, R16 (2001).
 - ²⁸ L. Kronik and Y. Shapira, *Surface Science Reports* **37**, 1 (1999).
 - ²⁹ D. K. Schroder, *Semiconductor Material and Device Characterization* (Wiley Interscience, New York, 1998).
 - ³⁰ S. Sze, *Physics of Semiconductor Devices* (John Wiley and Sons, New York, 1981).
 - ³¹ M. S. Tyagi and R. Van Overstraeten, *Solid-State Electronics* **26**, 577 (1983).
 - ³² A. G. Aberle, S. Glunz, and W. Warta, *Journal of Applied Physics* **71**, 4422 (1992).
 - ³³ This device was grown using an iron nitrate catalyst at 900°C, with 500 sccm hydrogen, 1000 sccm methane, and 20 sccm ethylene.
 - ³⁴ S. Heinze, J. Tersoff, and Ph. Avouris, *Applied Physics Letters* **83**, 5038 (2003).
 - ³⁵ J. Appenzeller, J. Knoch, V. Derycke, R. Martel, S. Wind, and Ph. Avouris, *Physical Review Letters* **89**, 126801 (2002).
 - ³⁶ T. Durkop, S. A. Getty, E. Cobas, and M. S. Fuhrer, *Nano Letters* **4**, 35 (2004).
 - ³⁷ G. Pennington and N. Goldsman, *Physical Review B* **68**, 045426 (2003).